Renewable Energy 38 (2012) 16–30

Contents lists available at ScienceDirect

Renewable Energy

journal homepage: www.elsevier.com/locate/renene

Unrestricted wind farm layout optimization (UWFLO): Investigating key factors influencing the maximum power generation

Souma Chowdhury [a], Jie Zhang [a], Achille Messac [b,*], Luciano Castillo [c]

[a] Department of Mechanical, Aerospace, and Nuclear Engineering, Rensselaer Polytechnic Institute, Troy, NY 12180, USA
[b] Department of Mechanical and Aerospace Engineering, Syracuse University, Syracuse, NY 13244, USA
[c] National Wind Resource Center, Department of Mechanical Engineering, Texas Tech University, Lubbock, TX 79409, USA

ARTICLE INFO

Article history:
Received 7 December 2010
Accepted 20 June 2011
Available online 17 August 2011

Keywords:
Farm layout
Particle swarm optimization
Turbine
Wake model
Wind energy

ABSTRACT

A new methodology, the Unrestricted Wind Farm Layout Optimization (UWFLO), that addresses critical aspects of optimal wind farm planning is presented in this paper. This methodology simultaneously determines the optimum farm layout and the appropriate selection of turbines (in terms of their rotor diameters) that maximizes the net power generation. The farm layout model obviates traditional restrictions imposed on the location of turbines. A standard analytical wake model has been used to account for the velocity deficits in the wakes created by individual turbines. The wind farm power generation model is validated against data from a wind tunnel experiment on a scaled down wind farm. Reasonable agreement between the model and experimental results is obtained. The complex nonlinear optimization problem presented by the wind farm model is effectively solved using constrained Particle Swarm Optimization (PSO). It is found that an optimal combination of wind turbines with differing rotor diameters can appreciably improve the farm efficiency. A preliminary wind farm cost analysis is performed to express the cost in terms of the turbine rotor diameters and the number of turbines in the farm. Subsequent exploration of the influences of (i) the number of turbines, and (ii) the farm land size, on the cost per Kilowatt of power produced, yields important observations.

1. Introduction

Renewable energy resources, particularly wind energy, have become a primary focus in Government policies, in academic research and in the power industry. The horizontal axis wind turbine is the most popular of its kind, which has been in existence since the 13th century [1]. The practical viability of given energy sources is generally governed by such factors as the potential for large scale energy production and the return on investment. These factors have been restraining the exploitation of the full potential of wind energy. The 2009 worldwide nameplate capacity of wind powered generators was only approximately 2% of the worldwide electricity consumption [2]. This calls for improvement in wind power generation technology, which can be realized in part through optimal planning of wind farms.

1.1. Wind farm optimization (WFO)

Wind energy resources generally appear in the form of wind farms that consist of multiple wind turbines located in a particular arrangement over a substantial stretch of land (onshore) or water body (offshore). It has been shown that the total power extracted by a wind farm is significantly less than the simple product of the power extracted by a standalone turbine and the number of identical turbines (N) in the farm [3]. Comparison of (i) the product of the power curve of a standalone turbine and N, and (ii) the power curve of the whole wind farm (Park Power Curve (PPC)) reveals this phenomenon. The discrepancy is 12.4% (which is the loss in farm efficiency) in the case of an offshore wind farm in Denmark [3].

This deficiency can be attributed to the loss in the availability of energy due to wake effects – i.e. the shading effect of a wind turbine on other wind turbines downstream from it [4]. The energy deficit due to mutual shading effects is determined using wake models that give a measure of both the growth of the wake, and the velocity deficit in the wake with distance downstream from the wind turbine. The Park wake model, originally developed by Jensen [5] and later by Katic et al. [6], is one of the most popular analytical wake models used in wind farm modeling. The modified Park wake model and the Eddy Viscosity wake model are other standard wake models. The reduction in the wind farm efficiency (loss in the effective energy available), due to this mutual shading, depends primarily on the geometric arrangement of wind turbines in a farm. Economic profit from a wind farm is one of the guiding factors in

* Corresponding author. Tel.: +1 315 443 2341.
E-mail address: messac@syr.edu (A. Messac).

0960-1481/$ – see front matter © 2011 Elsevier Ltd. All rights reserved.
doi:10.1016/j.renene.2011.06.033

planning a wind energy project, which in turn depends on the farm efficiency. Hence, an optimal layout of turbines that ensures maximum farm efficiency is expected to be important in conceiving a wind farm project.

Notable work has been done in layout optimization of wind farms. For instance, the Offshore Wind Farm Layout Optimization (OWFLO) project [7] seeks to minimize the Cost of Energy (COE) of the wind farm. The OWFLO software uses the PARK wake model [6], but also has the flexibility to use other wake models. Both, gradient based and evolutionary algorithms have been used for optimization purposes. The Danish PSO programme used the software WindPRO for wind farm layout analysis [3]. WindPRO is capable of implementing various wake models, such as Jensen's model [5], EWTS II and eddy viscosity model [8]. Beyer et al. [4] used the Riso Farm model, in conjunction with genetic algorithm to optimize the wind farm layout for maximum economic profit. Several other genetic algorithm based approaches have also been reported in the literature [9–11].

Kusiak and Zheng [12] presented an advanced layout optimization technique that uses evolutionary strategy algorithms. Array-like or grid-wise turbine locating restrictions have been avoided in the evolutionary strategy based technique [12]. Kusiak and Zheng [12] also provided an industrial case study involving different numbers of turbines (ranging from 2 to 6). Another interesting wind farm layout optimization model that uses an integer coded evolutionary algorithm, was recently published by Gonzaleza et al. [13]. The evolutionary algorithm based model [13] maximizes the net present value (NPV) of the wind farm initial capital investment. Gonzleza et al. [13] successfully account for factors such as partial wake-rotor overlap and terrains with non-uniform load bearing capacity soil. In the paper by Gonzleza et al. [13], critical commercial factors are also taken into consideration in modeling the net present value (NPV) of the wind farm life cycle cost.

1.2. Limitations of the existing WFO models

As discussed in the previous section, wind farm layout modeling approaches can be broadly classified into: (i) models that assume an array like (row-column) farm layout [3,14], and (ii) models that divide the wind farm into a discrete grid to search for the optimum grid locations of turbines [4,10,11,13]. The array-layout technique generally optimizes the lateral distance between each turbine (in a row) and the distance between the different rows of turbines. However, since the farm layout pattern is restricted (to arrays), this approach is likely to introduce an appreciable source of sub-optimality. The grid-wise locating scheme does tend toward an unrestricted farm layout approach, if the grid-size is of the order of the turbine rotor diameters. However, such a scheme yields a mixed-discrete nonlinear optimization problem with a high number of discrete variables (for a commercial farm with a large number of turbines), which often demands excessive computational resources in order to converge. In addition, the grid-wise locating scheme is not immediately applicable to wind farms of different shapes (other than the rectangular shape). In the UWFLO model developed in this paper, these limiting assumptions have been avoided. This unrestricted layout modeling approach is similar to the method presented by Kusiak and Zheng [12].

The induction factor of a turbine provides a measure of the energy drop in the wind, when the wind flows across the turbine. In the case of commercial wind turbines, the induction factor depends on the tip speed ratio of the turbine and the velocity of the incoming wind. Most of the popular wind farm power generation models (including recent models [12,13]) adopt a constant value of the induction factor over the entire wind farm. In the present study, a variable induction factor, dependent on the incoming wind velocity (for a given tip speed ratio), has been employed. In addition to the above-stated limitations, existing approaches generally confine the layout optimization study to wind farms comprised of identical wind turbines. However, in planning a wind farm, an appropriate combination of different types of turbines might prove to be economically more beneficial than using identical wind turbines. The UWFLO model, in conjunction with a preliminary wind farm cost model, is used to explore the benefits of using turbines with differing rotor diameters.

Existing analytical power generation models, including UWFLO, make significant assumptions and approximations in modeling the wake velocity deficit. These assumptions can lead to results that may not appropriately represent the commercial wind farm scenario. A Computational Fluid Dynamics (CFD) model is likely to achieve a more accurate estimation of the wake velocities, as performed by Cal et al. [15] using Large Eddy Simulation. However, a high fidelity CFD simulation of wind flowing across an entire wind farm would involve excessive computational complexity and process runtime.

1.3. Development of the UWFLO model

The Unrestricted Wind Farm Layout Optimization (UWFLO) model, presented in this paper is an extension of the UWFLO model, introduced by Chowdhury et al. [16]. In the UWFLO model, the growth of the wake behind a turbine is determined using the wake growth model proposed by Frandsen et al. [17]. The corresponding energy deficit behind a turbine is determined using the velocity deficit model originally presented by Katic et al. [6]; this velocity deficit model has been widely adopted in wind farm modeling [7,11,13]. In a wind farm, the velocity of the wind approaching a turbine can be affected by the wake of multiple turbines upstream from it. Crespo et al. [18] provide a review of different methods that account for the merging of wakes (wake superposition), in determining the wake velocity deficits. UWFLO implements the wake superposition model developed by Katic et al. [6]. The possibility of a turbine being partially in the wake of another turbine (upwind) has also been taken into account in the UWFLO power generation model.

The wind farm model developed in UWFLO is first validated against recently published experimental data [15]. In this wind tunnel experiment, the velocity distributions within a 3×3 array of model wind turbines are analyzed using a stereo PIV system. The power generated by the last row center turbine has also been determined for different incoming wind velocities. We perform layout optimization on a wind farm similar to that in the experimental setup [15], in terms of (i) the farm dimensions, (ii) the total number of turbines involved (nine), (iii) the surface roughness (farm topography), and (iv) the incoming wind conditions (averaged). The net power generated by the wind farm is evaluated by the sum of the power generated by the individual turbines. The farm dimensions and the minimum distance required between any two turbines are treated as system constraints. This UWFLO model represents a nonlinear continuous optimization problem; this problem is likely to be computationally less expensive to solve compared to the nonlinear mixed discrete-continuous problems, developed in the standard grid-wise locating approaches.

A Particle Swarm Optimization algorithm [19] is employed to optimize the farm layout with the objective of maximizing the total power generation. A robust constraint handling technique, based on constraint dominance principles [20], is employed to deal with the problem constraints. It was found from preliminary exploration that the design domain of the wind farm model has multiple local optima. PSO, being a stochastic search algorithm, deals with multimodal problems significantly better than do gradient based algorithms. Moreover, PSO is relatively simple to implement and

involves fewer user-defined parameters that need to be adjusted, compared to most other standard evolutionary optimization algorithms.

Such factors as (i) the use of turbines with differing rotor diameters, (ii) the number of turbines in a farm, and (iii) the farm land size are expected to play important roles in deciding the optimum farm layout. Further studies are performed using the UWFLO technique to investigate the influence of these factors. Two representative cost models (polynomial interpolations) are formulated to express the cost of a wind farm in terms of the turbine rotor diameter and the number of turbines in a farm. However, we could not analyze the relationship between the farm cost and the farm land size, owing to a lack of available data regarding the size of existing commercial wind farms. The authors point out that this paper does not intend to develop an extensive cost analysis of commercial wind farms; the actual cost depends on other important factors as well, which are not explicitly considered in this paper.

The following assumptions are made in the development of the overall UWFLO framework in this paper:

1. The designed wind farm is assumed to have a rectangular shape. This assumption is helpful for validating the UWFLO model against the data from the wind tunnel experiment (on a scaled down rectangular wind farm).
2. The incoming wind is assumed to be unidirectional and approaching witha fixed speed.
3. The analytical wake model [17] used in this paper assumes that, (i) the velocity inside the wake is axi-symmetric and uniform, (ii) the wake starts expanding immediately behind the turbine, and (iii) the freestream velocity is uniform. In addition, the wake flow speed profile is assumed to be self-similar [17]. The entrainment parameter is determined empirically and depends on the structure of turbulence.
4. In a commercial-scale wind farm, the relative placement of the turbines is also regulated by such factors as (i) the dynamic loading on the turbines, (ii) the local terrain, (iii) the load bearing capacity of the soil, and (iv) the road layout of the farm [13]. However, these additional practical constraints to the farm layout have not been considered in this paper.
5. In this paper the turbines in the wind farm are assumed to have the same hub height and the same performance characteristics.
6. In this paper, we develop two independent wind farm cost models, based on the turbine rotor diameters and the number of turbines installed. The cost of a wind farm is, however, a complex function that also depends on several other economic and environmental factors (e.g. labor costs, grid connection, site accessibility, turbine reliability, and Government policies).

Specific assumptions made in the component models that comprise the UWFLO framework, particularly the analytical power generation model, are stated in the course of the model formulation. The following topics are discussed in Sections 2–6, respectively: (i) the formulation of the power generation model; (ii) the formulation of the wind farm cost model; (iii) the validation of the model using the wind tunnel experiment data; (iv) a brief description of the PSO algorithm; and, (v) three case studies in wind farm layout optimization.

2. Unrestricted wind farm layout optimization (UWFLO) model

2.1. Analytical power generation model

The power generated by a wind farm is an intricate function of the configuration and location of the individual wind turbines. The flow pattern inside a wind farm is complex, primarily due to the wake effects and the highly turbulent flow. It is helpful to determine the velocity of the wind approaching a turbine and the corresponding power generated separately for each turbine and in a particular order (based on the streamwise location). A wind farm of given dimensions, consisting of N turbines, is considered here. This wind farm is exposed to a wind profile [15] given by

$$\frac{U}{U_\infty} = b_1\left(\frac{z}{b_2}\right)^{0.15} \tag{1}$$

where U represents the wind velocity at a height z above the ground, U_∞ represents the freestream wind velocity, and b_1 and b_2 are constants that depend on the terrain, the surface roughness and the atmospheric conditions. However, in this paper we assume a uniform incoming flow (defined by the velocity, U_0) equivalent to the velocity (in Eq. (1)) integrated and averaged over the rotor area. We determine the total power generated by the wind farm by observing the following sequence of five steps.

Step 1. Each turbine is assigned a coordinate (X, Y) based on a fixed coordinate system (X_i, Y_i). This system is then transformed into another coordinate system (x, y), such that the positive x-direction is aligned with the current direction of the wind (constant or variable) using

$$\begin{bmatrix} x_i \\ y_i \end{bmatrix} = \begin{bmatrix} \cos\theta & -\sin\theta \\ \sin\theta & \cos\theta \end{bmatrix} \begin{bmatrix} X_i \\ Y_i \end{bmatrix} \tag{2}$$

In Eq. (2), θ is the angle made by the direction of the wind with the positive X-axis when measured clockwise. The separation between any two turbines (i and j) is denoted by

$$\Delta x_{ij} = x_i - x_j, \quad \Delta y_{ij} = y_i - y_j \tag{3}$$

Step 2. In order to identify whether a turbine is within the influence of the wake of another turbine, an influence matrix M is created such that,

$$M_{ij} = \begin{cases} +1 \text{ if Turbine} - i \text{ influences Turbine} - j \\ -1 \text{ if Turbine} - j \text{ influences Turbine} - i \\ 0 \text{ if there is no mutual influence} \end{cases} \tag{4}$$

where Turbine-j is in the influence of the wake created by Turbine-i if and only if

$$\Delta x_{ij} < 0 \quad \& \quad \left|\Delta y_{ij}\right| - \frac{D_j}{2} < \frac{D_{\text{wake},ij}}{2} \tag{5}$$

where D_j is the rotor diameter of Turbine-j and $D_{\text{wake},ij}$ is the diameter of the wake front due to Turbine-i, approaching Turbine-j.

Step 3. The turbines are ranked ($R_i = 1,2,\ldots,N$) in the increasing order of their x-value. Thereby, the closer the turbine is to the direct wind (wind entering the farm) the lower its rank. If any two turbines have the same x -coordinate, they will be assigned the same rank.

Step 4. The power generated by each turbine (say Turbine-j) is computed sequentially in the order of its rank, i.e. starting with rank one. This method ensures that the influence of the wakes (both individual and merged) from the turbines upwind can be appropriately accounted for. Turbine-j might be partially or completely in the wakes of other turbines. The wake of each preceding turbine (say Turbine-k) for which $M_{kj} = 1$, is mapped onto Turbine-j as follows:

- If the rotor of Turbine-j is completely in the wake of Turbine-k, then

$$A_{kj} = A_j \\ A_j = \pi D_j^2/4 \tag{6}$$

- If the rotor of Turbine-j is partially in the wake of Turbine-k, then

$$A_{kj} = r_k^2\cos^{-1}\left(\frac{d_{kj}^2+r_k^2-r_j^2}{2d_{kj}r_k}\right) + r_j^2\cos^{-1}\left(\frac{d_{kj}^2+r_j^2-r_k^2}{2d_{kj}r_j}\right) - \frac{1}{2}\sqrt{\left(-d_{kj}+r_k+r_j\right)\left(d_{kj}-r_k+r_j\right)\left(d_{kj}+r_k-r_j\right)\left(d_{kj}+r_k+r_j\right)} \tag{7}$$

where A_{kj} is the effective area of influence of the wake (from Turbine-k) on Turbine-j. The terms r_k and r_j are the areas of the wake front and the Turbine-j rotor (the circles in Fig. 1), respectively; and d_{kj} is the distance between the two centers.

The contribution of the wake of each upwind Turbine-k (P_{kj}) toward the net kinetic energy approaching Turbine-j per unit time is given by

$$P_{kj} = \frac{A_{kj}}{A_j}U_{kj}^2 \tag{8}$$

where U_{kj} is velocity of the wake produced by Turbine-k and approaching Turbine-j. The effective deficit, in the velocity of the wind approaching Turbine-j, can be estimated as the quadratic sum of the deficits of all the influencing turbines (all Turbine-k's with $M_{kj} = 1$) [6,13]. The corresponding velocity of the wind approaching Turbine-j is expressed as

$$U_j = U_0 - \sqrt{\sum_k \frac{A_{kj}}{A_j}\left(U_0 - U_{kj}\right)^2} \quad \forall \ k \text{ yielding } M_{kj} = 1 \tag{9}$$

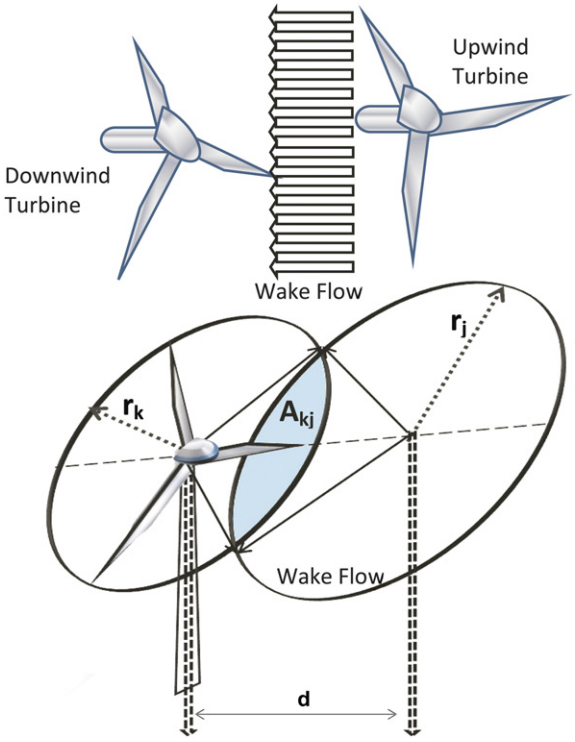

Fig. 1. Overlap of a wake front and a turbine rotor.

The power P_j, generated by Turbine-j, is then determined using the formula

$$P_j = k_g k_b C_p'\left(\frac{1}{2}\rho\pi\frac{D_j^2}{4}U_j^3\right) \tag{10}$$

where ρ is the density of air. The parameters k_g and k_b are the generator efficiency (electrical efficiency) and the gearbox efficiency (mechanical efficiency), respectively. The parameter C_p' is the coefficient of power, which is a measure of the ratio of power extracted from the wind and the power available. The power coefficient is characteristic of the design of the turbine rotor and is dependent on the tip speed ratio and the incoming wind velocity. The maximum achievable value of C_p' is 0.59, which is given by the Betz limit [21]. In the remainder of the paper, the product of the efficiencies and the parameter C_p' will be referred to as the power coefficient C_p that is

$$C_p = k_g k_b C_p' \tag{11}$$

Step 5. The power generated by the farm, P_{farm}, is given by the algebraic sum of the powers generated by the individual turbines, which is expressed as

$$P_{\text{farm}} = \sum_{j=1}^{N} P_j \tag{12}$$

Accordingly, the farm efficiency [3] can be expressed as

$$\eta_{\text{farm}} = \frac{P_{\text{farm}}}{\sum_{j=1}^{N} P_{0j}} \tag{13}$$

where P_{0j} is the power that Turbine-j would generate if operating as a standalone entity, for the given uniform incoming wind speed. However, owing to the nature of the power curve for the experimental model-turbines (discussed in Section 4.1), the above expression can yield farm efficiencies higher than one. In order to avoid this apparent anomaly, the effective farm efficiency $\overline{\eta}_{\text{farm}}$ is defined as

$$\overline{\eta}_{\text{farm}} = \frac{P_{\text{farm}}}{\sum_{j=1}^{N} P_{Rj}} \tag{14}$$

where P_{Rj} is the rated power for Turbine-j. In the case of the experimental model-turbines, the rated power is estimated to be 0.385 W (Fig. 4).

2.2. Wake model

The wake model used in UWFLO, which determines the growth of individual wakes has been adopted from Frandsen et al. [17]. This model employs the control volume concept that relates the thrust and power coefficients to the velocity deficit [21,22]. The growth of the wake front behind any Turbine-j is given by the equation

$$D_{\text{wake},j} = (1+2\alpha\bar{s})D_j, \quad \text{where} \\ \bar{s} = s/D_j \tag{15}$$

where $D_{\text{wake},j}$ is the diameter of the expanding wake front at a distance s behind Turbine-j. The parameter α is the wake spreading constant [17], which is determined using the formula

$$\alpha = \frac{0.5}{\ln\left(\frac{z_H}{z_0}\right)} \tag{16}$$

where z_H and z_0 are the average hub height of the turbines and the average surface roughness of the wind farm region, respectively. The wind velocity in the wake [6] is given by

$$U = \left(1 - \frac{2a}{(1+2\alpha s)^2}\right) U_j \tag{17}$$

where a is the induction factor, which can be determined from the coefficient of thrust (C_t). The latter is one of the design characteristics of a turbine rotor. Eq. (17) is equivalent to the expression suggested in the Park wake model [5,6].

3. UWFLO cost model

Numerous techniques have been developed to evaluate the cost (installation, operation and maintenance) of both onshore and offshore wind farms over the past twenty years. Notable examples include: the short-cut model [23], the cost analysis model for the Greek market [24], the OWECOP-Prob cost model [25], the JEDI-wind cost model [26], and the Opti-OWECS cost model [27]. Among these cost models, only Refs. [23,24] present analytical expressions of the cost as functions of the critical contributing factors. Turbine-rotor diameters strongly affect the flow pattern inside the wind farm, and thereby influences the performance and the net economy of the farm. Most of the existing models do not explicitly consider the effect of the rotor diameter of the wind turbines. Generally, only the rated power of the wind turbines is considered as a variable in these cost models. A new response surface based cost model developed by Zhang et al. [28] explains how the rotor diameter of the turbines installed is a crucial factor in determining the Cost of Energy (COE) of a wind farm.

In this study, quadratic response surfaces have been developed to represent the cost of a wind farm. A general m-variable quadratic response surface is expressed as

$$Cost = c_0 + \sum_{i=1}^{m} c_i v_i + \sum_{i=1}^{m} c_{ii} v_i^2 + \sum_{i=1}^{m} \sum_{\substack{j=1 \\ j \neq i}}^{m} c_{ij} v_i v_j \tag{18}$$

where the v_i's and the c_i's respectively denote the generic variables and the unknown coefficients. These coefficients are determined through the least squares approach, using available commercial data. Two single variable response surfaces have been developed in this paper. One expresses the cost of a wind farm as a function of the turbine rotor diameter, and the other expresses the wind farm cost as a function of the number of turbines in the farm. The cost functions in this paper represent the cost per KW of installed capacity (total rated capacity of the wind farm). The rotor diameter based cost function is developed to allow for an unbiased comparison of the performance of wind farm designs with different combinations of turbine rotor diameters. The number of turbines based cost function is developed to specifically explore and compare the variations in (i) the total power generation and (ii) the cost of a wind farm with the installed number of turbines. These functions are evaluated using data for wind farms in the state of New York, provided by the Wind and Hydropower Technologies program (US Department of Energy) [26].

The farm cost functions are developed using data [26] on different 1.5 MW turbines. The estimated rotor diameter based cost function is given by

$$Cost_D(D) = 143.85 - 0.32447D - 1.4841\times10^{-3}D^2 \tag{19}$$

where D is the diameter of the wind turbines in the farm. The cost function in Eq. (19) was evaluated with a relative error of 0.2%. Sufficient cost information is not available for commercial wind farms with non-identical wind turbines (turbines with differing rotor diameters). Therefore, the cost of a wind farm with non-identical wind turbines is approximated by

$$Cost_D(D_1, D_2, \ldots, D_N) = \frac{1}{N}\sum_{j=1}^{N} Cost(D_j) \tag{20}$$

The number of turbines based cost function (considering identical wind turbines) is given by

$$Cost_N(N) = 133.3938 - 0.1501N - 7.9\times10^{-4}N^2 \tag{21}$$

The cost function in Eq. (21) was evaluated with a relative error of 0.21%. In this case, the effective cost per KW of power produced ($Cost_{N,\text{eff}}$) can be expressed as

$$Cost_{N,\text{eff}} = \frac{Cost_N \times P_0 \times N}{P_{\text{farm}}} \tag{22}$$

As stated in Section 1, the economics of a wind farm depend on a series of environmental, technical and financial factors, which have not been explicitly accounted for in this paper. However, the objectives of the 1D quadratic cost models in Eqs. (20) and (22) are to, respectively, explore (i) the benefits of using non-identical turbines and (ii) the influence of "the number of turbines installed" on the net economic utility of a wind farm. Specifically, we break more ground in exploring the potential impacts of these factors. These cost functions are highly sensitive to the training data used. Considering the likely uncertainties in various economic factors related to wind energy, these functions might not readily apply to the broad commercial scenario in wind farm cost modeling. Future research should pursue the development of more comprehensive wind farm cost models.

4. Power generation model validation

4.1. Wind tunnel experiment [15]

Experimental measurements are used to validate the power generation model in UWFLO. The experiment consists of a scaled down wind farm that is placed in a wind tunnel as shown in Fig. 2. A 3 × 3 array of model wind turbines was subjected to inflow conditions that represent those of a neutrally stable boundary layer flow. Hot-wire anemometry was used to characterize the inflow properties. Measurements of the flow inside the array were performed using Stereo-Particle Image Velocimetry in 18 planes surrounding the center wind turbine of the third row, downstream. In the remainder of the paper this wind turbine is referred to as the Turbine-8. Detailed information, regarding the experiment, can be found in the paper by Cal et al. [15].

The properties of the wind farm and the incoming wind characteristics are given in Tables 1 and 2, respectively. The mean velocity profile [15] in meters per second is given by

$$\frac{U(y)}{U_\infty} = 8.4\left(\frac{y}{0.37}\right)^{0.15} \tag{23}$$

The variation of the power coefficient (C_p) with streamwise velocity was determined from direct torque measurements performed on Turbine-8. Extensive details of these measurements has been provided by Kang et al. [29]. The C_p curve presented in Fig. 3 corresponds to a constant tip speed ratio (λ) of 4.9, which was used during the experiments. Three operational points were measured and a quadratic curve fit was obtained.

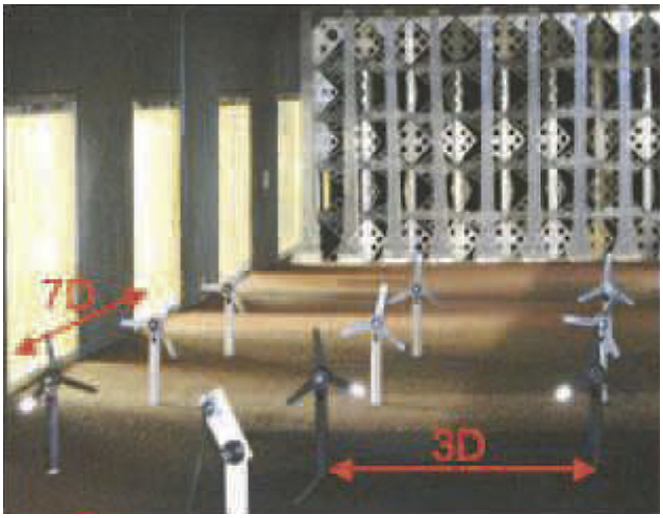

Fig. 2. Photograph of the experimental setup from a downstream location [15].

The loss in velocity incurred by the wind, while flowing across a turbine, is generally characteristic of the turbine design and control. A measure of this velocity loss is given by the induction factor a that is defined as

$$a = 0.5\left(1 - \frac{U_{\text{back}}}{U_{\text{front}}}\right) \tag{24}$$

where U_{front} and U_{back} are respectively the average streamwise velocities of the wind in front of and behind the turbine, each of which has been modeled as a streamtube that passes through a rotor disk. According to the 1-dimensional ideal flow assumption [30], the induction factor and the coefficient of power are related by

$$C_p = 4a(1-a)^2 \tag{25}$$

Eq. (25) is solved to yield the values of the induction factor (a), using the measured values of C_p. Fig. 3(b) shows the corresponding quadratic fit obtained for the variation of the induction factor with the incoming wind velocity. However, beyond the boundary data point (point A in Fig. 3(b)), the induction factor curve is approximated using a linear extrapolation (dashed line in Fig. 3(b)) to compensate for the lack of information over a wide range of velocities. The slope of this linear extrapolation is set to be equal to that of the quadratic function at the boundary point. This approximation was necessary because several wind turbines (both during validation of the model and optimization) were observed to operate in the velocity range of 5.2–7.1 m/s.

In the case of the experimental conditions, the induction factor (for Turbine-8) evaluated from Eq. (25) is $a \simeq 0.05$, while that directly measured from the flow field is $a = 0.087$. This underestimation can be attributed to the ideal flow assumption that neglects critical factors such as (i) rotor inefficiencies, (ii) wake of the tower, and (iii) existence of the hub. Detailed information regarding the calculation of the induction factor from the velocity field may be found in Ref. [31]. It is seen from Fig. 3(a) and (b) that the maximum values of C_p and a (0.3125 and 0.095, respectively) occur at a velocity of 5.00 m/s.

Fig. 4 shows the variation of the actual power generated by a wind turbine as a function of the incoming wind velocity. The available wind energy increases with velocity, whereas the extent to which it can be extracted by the turbine (represented by C_p) may follow a different trend, compared to that shown in Fig. 3(a). As a result, the power curve (Fig. 4) offers a more explicit representation of the actual performance of wind turbines. It is seen that the maximum power ($P = 0.385$ W) is generated when the approaching wind velocity is 6.17 m/s.

Table 1
Wind farm properties.

Attribute	Value
Length	1.68 m
Breadth	0.72 m
Turbine hub height (H)	0.12 m
Turbine rotor diameter (D)	0.12 m
Downwind separation	$7 \times D$ m
Crosswind separation	$3 \times D$ m
Average surface roughness	0.001 m

Table 2
Wind characteristics.

Parameter	Value
Rotor averaged wind speed (U_0)	7.09 m/s
Mean velocity profile	Refer Eq. (23)
Wind direction	0° with positive X-axis
Density of air	1.2 kg/m^3

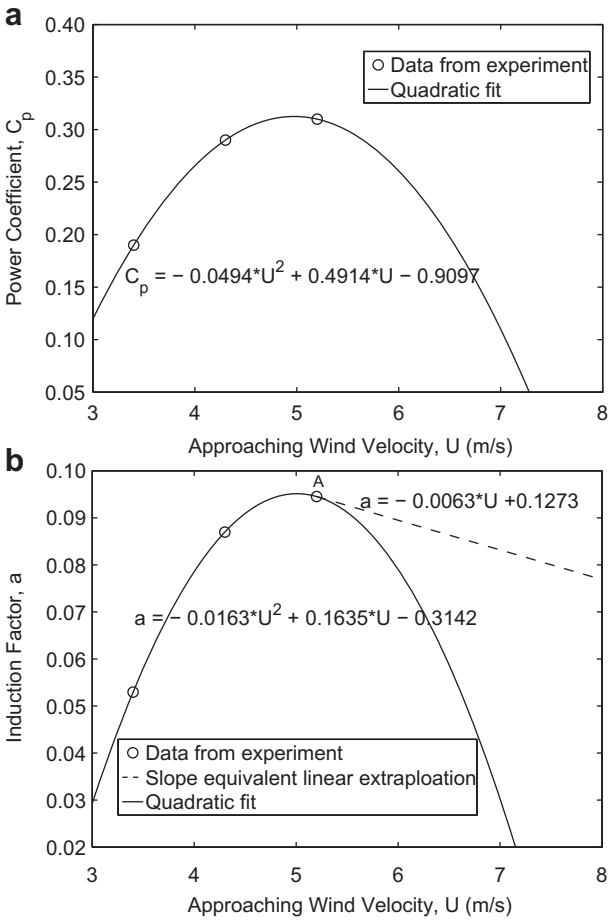

Fig. 3. (a) Coefficient of power (C_p) curve. (b) Induction factor, a, curve.

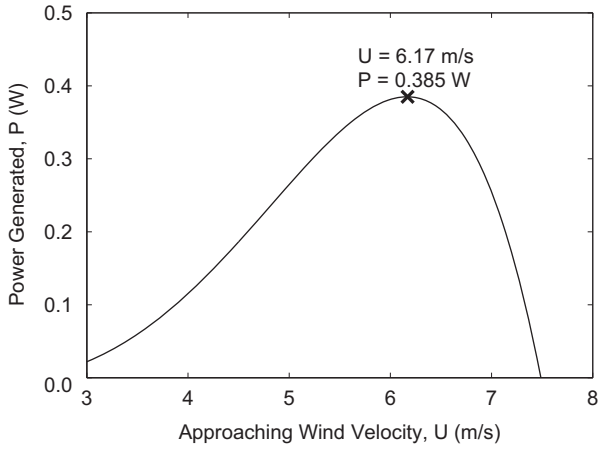

Fig. 4. Power curve for the experimental wind turbines.

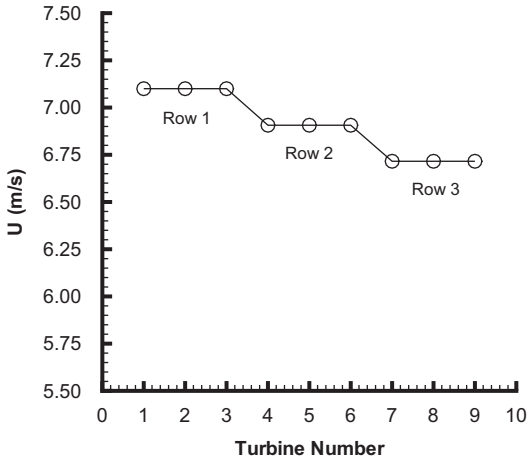

Fig. 6. Velocity of wind approaching each turbine (determined by the model).

4.2. Model validation results

The wind farm is assumed to be exposed to a unidirectional wind blowing in the positive X direction, as in the case of the experimental setup [15]. The configuration of the wind farm simulated in the model is a near replica of the wind farm experiment, and the input data used is derived from Tables 1 and 2. One difference between the UWFLO model and the experiments is that the inflow conditions in the model represent a uniform flow without turbulence. A rotor-averaged inflow velocity of 7.09 m/s is used in the model, which is similar to the conditions maintained in the experiment.

The coefficient of power, $C_{p,}$ and the induction factor, a, are determined using Eqs. (11) and (24), respectively. $C_{p,\max}$ is evaluated to be 0.3125. The arrangement of turbines in the experiment is shown in Fig. 5. The dashed line rectangle represents the boundary of the wind farm and the numbered squares represent the turbine locations. The velocity of the wind approaching each turbine, the corresponding power available, and the power generated in the case of each turbine are shown in Figs. 6, 7(a) and (b) , respectively.

In the experiment, extensive measurements of different parameters are made for Turbine-8 (last row, center turbine). Table 3 compares the values of these key parameters obtained using the model with the experiment measurements. It is seen from Fig. 6 and Table 3 that the model overestimates the velocity of the wind immediately in front of the last row center turbine (Turbine-8) by 7.53%. This difference can be attributed to the various assumptions made in the analytical wake model used; namely (i) uniform flow, (ii) no explicit consideration of turbulence, and (iii) the disregard of factors such as rotor inefficiencies and other wake model inaccuracies. However, the general trend of

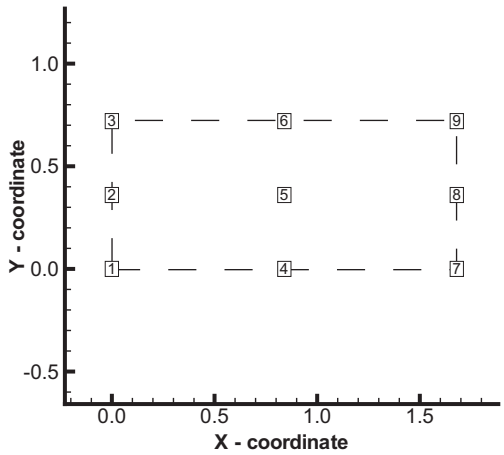

Fig. 5. Wind farm layout in the experiment [15] (dimensions in meters).

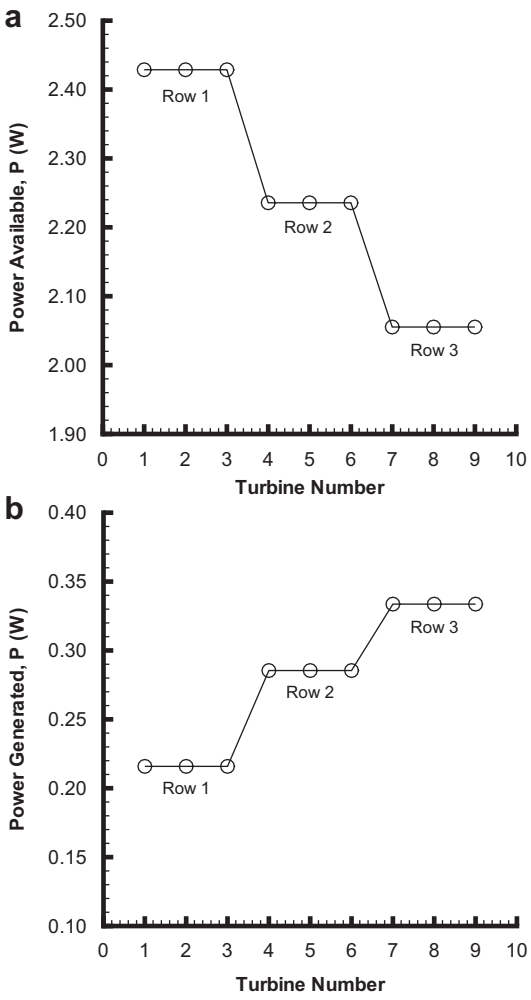

Fig. 7. (a) Power available for each turbine. (b) Power generated by each turbine.

Table 3
Comparison of the power generation model with the experiment.

Parameter	Wind farm model	Experiment
U in front of turbine	6.71 m/s	6.24 m/s
Power generated	0.336 W	0.34 W
C_p	0.16	0.21
a	0.085	0.087

velocity deficit is appropriately captured by the model. Fig. 7(a) and (b) show that, although the power available from wind decreases downstream due to the wake effects, the power generated by each turbine follows an opposite trend. The model is also observed to underestimate the power generated by Turbine-8 (as seen from Fig. 7(b) and Table 3). These observations are explained by the overall nature of the power curve (Fig. 4). The incoming wind (at 7.09 m/s) in this case is already above the optimal/rated wind speed (6.17 m/s); therefore, with decreasing velocity downstream, the power generated increases. The total power generated by the farm (Eq. (12)) and the corresponding farm efficiency (Eq. (14)) are computed to be 2.53 W and 0.73, respectively. These computed data will be useful, when we compare the performance of the optimized wind farm with that of the 3×3 array wind farm. It is helpful to note that, the computed data used for validation and performance comparison is subject to the undesirable deviations (in the estimated velocity deficits), introduced by the assumptions in the analytical wake model.

Analytical wake models similar to that used in this paper provide a computationally inexpensive means of determining wind farm power generation. This attribute is particularly helpful for optimization, which may require iterative comparisons of a large number of wind farm designs. However, the inherent assumptions in these simplified wake models can often be a source of appreciable error in the farm power estimation. The development of wake models that provide a more attractive trade-off between (i) accuracy/reliability and (ii) computational expense would be helpful in addressing this issue.

In the authors' opinion, the reliability of the wake model (e.g. wake expansion, wake velocity deficit, and wake merging) is a key factor that governs the accuracy of the overall power generation model. The determination of the power generated by an individual turbine is also subject to the approximations made regarding the relationship between the power coefficient (C_p) and the incoming wind velocity. The likely errors attributed to these approximations can, however, be minimized if reliable power curves are available from commercial turbine manufacturers. The framework presented in this paper makes unique contributions in developing an "unrestricted farm layout design" protocol and exploring the use of differing turbine rotor diameters. The integration of advanced wake models and reliable turbine power characteristics would further advance the practical use of the UWFLO model.

5. Constrained particle swarm optimization (PSO) algorithm

PSO is one of the most well known stochastic optimization algorithms, initially coined by an Electrical Engineer (Russel Eberhart) and a Social Psychologist (James Kennedy) in 1995 [19]. Later, several improved variations of the algorithm have appeared in the literature and been used in popular commercial optimization packages. The PSO algorithm used in this project has been derived from the unconstrained version presented by Colaco et al. [32]. A general single objective constrained maximization problem can be expressed as

$$\begin{aligned} &\text{Max } f(X_{\text{var}}) \\ &\text{subject to} \\ &g_j(X_{\text{var}}) \le 0, \quad j = 1,2,\ldots,p \\ &h_k(X_{\text{var}}) = 0, \quad k = 1,2,\ldots,q \end{aligned} \tag{26}$$

where p and q are the number of inequality and equality constraints, respectively, and X_{var} is the vector of design variables. The basic steps of the algorithm are summarized as

$$\begin{aligned} x_i^{t+1} &= x_i^t + v_i^{t+1} \\ v_i^{t+1} &= \alpha v_i^t + \beta_l r_1 (p_i - x_i^t) + \beta_g r_2 \left(p_g - x_i^t\right) \end{aligned} \tag{27}$$

where,

- x_i^t is *ith* member of the population (swarm) at the *tth* iteration,
- r_1 and r_2 are random numbers between 0 and 1,
- p_i is the best candidate solution found for the *ith* member,
- p_g is the best candidate solution for the entire population, and
- α, β_l and β_g are user-defined constants.

The technique used to deal with constraints is based on the principle of constrained non-domination, introduced by Deb et al. [20] and later adopted by Chowdhury et al. [33]. In this technique, solution-*i* is said to dominate solution-*j* if,

- solution-*i* is feasible and solution-*j* is infeasible or,
- both solutions are infeasible and solution-*i* has a smaller constraint violation than solution-*j* or,
- both solutions are feasible and solution-*i* weakly dominates solution-*j*.

If none of the above conditions apply (possible only in the case of a multi-objective problem), then the solutions are considered non-dominated with respect to each other.

6. Application of the UWFLO framework

The UWFLO technique has been applied to three different layout optimization cases (1, 2 and 3) for different wind farm scenarios, as listed below.

Case 1. Wind farm with identical turbines (same rotor diameter).
Case 2. Wind farm with non-identical turbines (differing rotor diameters).
Case 3. Wind farm with identical turbines that can adapt to wind conditions, as in the case of commercial turbines.

The specified incoming wind velocities in Cases 1 and 2 are the same as in the experiment [15]. The specified incoming velocity in Case 3 is lower than that in the experiment [15]. Case 3 is further applied to investigate the influences of the number of turbines and the farm land size, on the optimal layout of the wind farm. All three cases assume a unidirectional wind of constant speed, since specific information regarding the distribution of wind speed and direction was not available for the experiment [15]. However, in the commercial scenario, the speed and the direction of wind change with time. In the literature [1], the long term wind speed variation is often represented using a Weibull distribution, which is controlled by the shape parameter K and the scale parameter C. The values of these parameters have not been reported in the case of the experimental setup [15]. Nevertheless, this assumption does not restrict the application of the UWFLO framework. When the annual distribution of wind speed and direction is available for a particular wind farm site, a numerical integration procedure can be readily

performed to approximate the overall energy production (as in Ref. [12]).

It is noteworthy that the optimum wind farm layout is not necessarily unique. There can be different optimal arrangements of turbines with nearly equal amount of total power output, which results in a multimodal optimization problem. To compensate for the performance fluctuations induced by the random number generators in PSO (used in creating the initial population and other swarm operators), the algorithm is run five times for each case.

6.1. UWFLO Case 1

In Case 1, the wind farm is comprised of a fixed number of identical wind turbines (with rotor diameter = D). The wind farm properties (except for the layout) and the nature of the incoming wind are the same as given in Tables 1 and 2. Also, the turbines are assumed to be always facing the incoming wind. The layout of the rectangular wind farm is optimized to achieve maximum power generation. The optimization problem is defined as

$$\begin{aligned} &\text{Max } f(V) = \overline{\eta}_{\text{farm}} \\ &\text{subject to} \\ &\quad g_1(V) \le 0 \\ &\quad V = \{X_1, X_2, \ldots\ldots, X_N, Y_1, Y_2, \ldots\ldots, Y_N\} \\ &\quad 0 \le X_i \le X_{\text{farm}} \\ &\quad 0 \le Y_i \le Y_{\text{farm}} \end{aligned} \tag{28}$$

where η_{farm} is given by Eq. (14). The inequality constraint g_1 represents the minimum clearance required between any two turbines, and is given by

$$\begin{aligned} g_1(V) &= \sum_{i=1}^{N} \sum_{\substack{j=1 \\ j \ne i}}^{N} \max\left((D_i + D_j + \Delta_{\min} - d_{ij}), 0\right) \\ d_{ij} &= \sqrt{\Delta x_{ij}^2 + \Delta y_{ij}^2} \end{aligned} \tag{29}$$

In Eq. (29), $\Delta_{\min}$ is the minimum clearance required between the outer edge of the rotors of the two turbines. The value of $\Delta_{\min}$ is set at zero, to allow maximum flexibility in turbine spacing. In practice, a higher value of $\Delta_{\min}$ is advisable. The parameters X_{farm} and Y_{farm} in Eq. (28) represent the dimensions of the rectangular wind farm in the X and Y directions, respectively. To ensure the placement of the wind turbines within the fixed size wind farm, the X_i and Y_i bounds are formulated into an inequality constraint, $g_2(V) \le 0$. The constraint g_2 is expressed by

$$\begin{aligned} g_2(V) = \frac{1}{2N}\Bigg(&\frac{1}{X_{\text{farm}}} \sum_{i=1}^{N} \max\Big(-X_i, X_i - X_{\text{farm}}, 0\Big) \\ &+ \frac{1}{Y_{\text{farm}}} \sum_{i=1}^{N} \max\Big(-Y_i, Y_i - Y_{\text{farm}}, 0\Big)\Bigg) \end{aligned} \tag{30}$$

In this optimization problem, the number of design variables (N_{var}) is equal to $2N$.

6.2. UWFLO Case 1 results

The objective of this study (Case 1) is to investigate the layout optimization of a wind farm that has the same properties, and is subjected to the same conditions as in the experiment [15]. Optimization is performed using the PSO algorithm, which is initiated with a population of random wind farm layouts. The user defined constants involved in PSO are summarized in Table 4. The outcomes of one of the representative runs for Case 1 are illustrated in this paper.

Table 4
User-defined constants in PSO.

Constant	Value
α	0.5
β_g	1.4
β_l	1.4
Population size	$5 \times N_{\text{var}}$
Allowed number of function calls	15000

Fig. 8 shows that the algorithm converges after approximately 3000 function evaluations during which the power generated by the farm increases by 15.54%. The power generated by the optimum farm layout (3.298 W) is 30.19% higher than that generated by the original farm layout in the experiment (Fig. 5). The increase in the power generated by the wind farm through unrestricted layout optimization is substantial. In the remainder of the paper, the farm layout obtained by UWFLO is referred to as the "optimum farm layout". It should be noted that, since we are using heuristic optimization, this method does not necessarily guarantee a global optimum. The optimum farm layout is shown in Fig. 9, and the power generated by each turbine (of this wind farm) is shown in Fig. 10. Fig. 10 presents the wind velocity immediately in front of each turbine. In the UWFLO model, the rank of the turbines that represents the order in which the turbines encounter the incoming wind. Fig. 10(a) and (b) are thus plotted with respect to the turbine number that is equivalent to the turbine rank. Thereby, a discrete manifestation of the variation of P and U in the downstream direction is provided.

The optimization procedure sought to arrange the turbines in a manner such that most of them operate near the maximum power generation point of the power curve (rated speed of 6.17 m/s, as seen from Fig. 4). This phenomenon can be observed from Fig. 10(a) and (b). The increase in the power generated by the turbines (as illustrated by 10(b)) as we move downstream (increasing turbine rank) might initially seem counterintuitive. However, this phenomenon can be attributed to the specific nature of the power curve for the experimental model-turbines (as shown in Fig. 4) - beyond the rated speed of wind, the power decreases with increasing speed. The incoming wind speed (which is 7.0896 m/s) in this case is greater than the rated wind speed. This condition leads to the deliberate positioning of certain turbines in the wakes of other turbines located upstream (as shown in Fig. 9), thereby facing an incoming wind speed that approaches the rated speed (through speed reduction). The above observation shows that this farm optimization methodology is appropriately adaptive

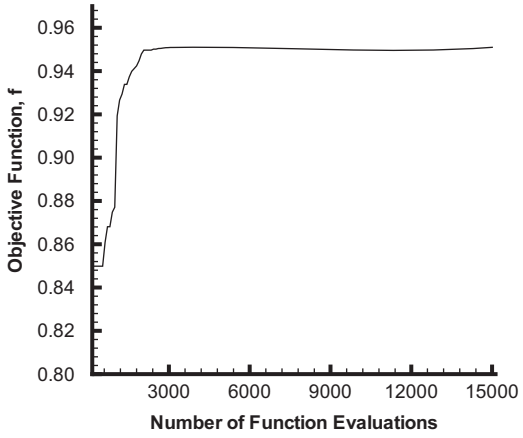

Fig. 8. Convergence history of PSO (Case 1).

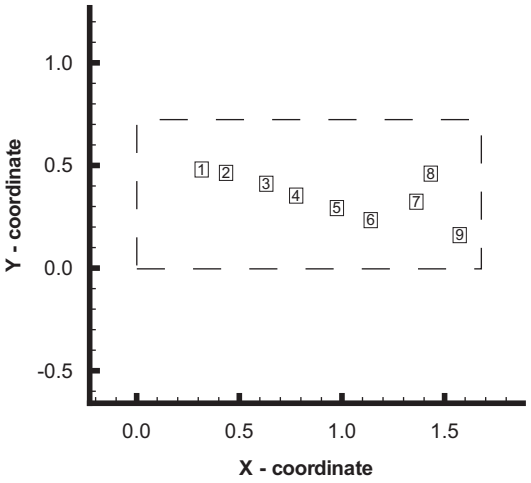

Fig. 9. Optimized wind farm layout in meters (Case 1).

to the input parameters such as turbine characteristics specified by the user.

Nevertheless, in the case of a commercial wind farm, the scenario may be quite different. This is because real life wind turbines are designed to orient themselves (such as by changing the pitch and yaw angle) in order to extract maximum power from the wind while operating within other constraints such as structural limitations. Hence, the power curve and the performance characteristics of real life wind turbines (details available in the Wind Energy Handbook [1]) are more complex than the simple "scaled down model-turbines" used in the experiment [15]. However, these performance characteristics are simply inputs to the UWFLO model. The optimization results illustrate how the UWFLO model is expected to produce reliable results for full scale commercial wind farms, when the appropriate performance curves are provided.

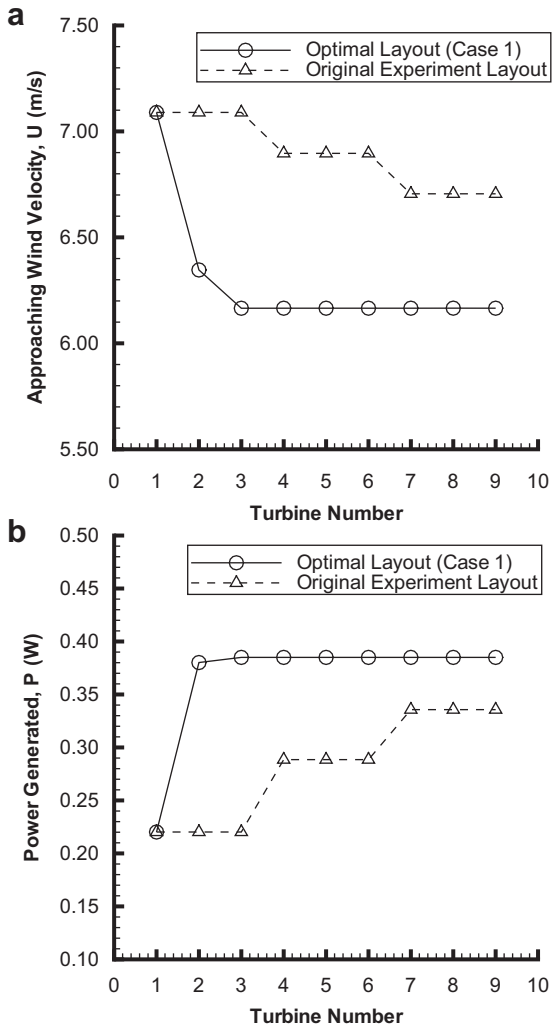

Fig. 10. (a) Velocity of wind approaching each turbine (U). (b) Power generated by each turbine (P).

6.3. UWFLO Case 2

In Case 2, the wind turbines are allowed to take on different rotor diameters. Other specified parameters in Case 2 are similar to those in Case 1 (refer Tables 1 and 2). During optimization, the rotor diameter of each turbine is treated as a design variable. Hence, there is a total of $3N$ design variables in Case 2, as opposed to $2N$ variables in Case 1. The rotor diameter based cost of a wind farm is implemented as an additional constraint g_3. This constraint is defined as

$$g_3(V) = \frac{1}{N}\sum_{i=1}^{N} Cost(D_i) - Cost_D(D_0) \tag{31}$$

where D_0 is a reference rotor diameter, which in this case is set equal to that of the experimental model-turbines. It should be noted that the objective function (effective farm efficiency) is defined with respect to the rated power of the experimental scale model-turbine (0.385W). In order to maximize the power generated by the wind farm, the optimization problem in Case 2 is formulated as

$$\begin{aligned}
&\text{Max } f(V) = \overline{\eta}_{\text{farm}}\\
&\text{subject to}\\
&\quad g_1(V) \le 0\\
&\quad g_2(V) \le 0\\
&\quad g_3(V) \le 0\\
&\quad V = \{X_1, X_2, \ldots\ldots, X_N,\ Y_1, Y_2, \ldots\ldots, Y_N,\ D_1, D_2, \ldots\ldots, D_N\}\\
&\quad 0 \le X_i \le X_{\text{farm}}\\
&\quad 0 \le Y_i \le Y_{\text{farm}}\\
&\quad D_{\min} \le D_i \le D_{\max}
\end{aligned} \tag{32}$$

6.4. UWFLO Case 2 results

The objective of this study (Case 2) is to explore the effect of using non-identical wind turbines (differing rotor diameters) on the total power generation from the wind farm. This investigation demands simultaneous optimization of the location and the rotor diameter of each turbine placed in the wind farm. The rotor diameter based cost constraint (g_3) ensures that any feasible wind farm design requires a net investment equal to or less than that required for a wind farm with identical wind turbines. The mean rotor diameter and the deviation in diameter, determined from the commercial data used for the cost function evaluation [26], are 75 m and 25 m, respectively. These commercial-scale design dimensions, when scaled down to the dimensions of the model turbines, used in the experiments (with $D = 0.12$ m), yield a deviation of 0.04 m. Thus, the feasible range of rotor diameter was specified as 0.08–0.16 m. However, in practice, only a limited set of choices of rotor diameters (for wind turbines) is commercially available. Hence, a more practical wind farm optimization calls for the treatment of rotor diameters as discrete design variables. This requirement has not been considered in this paper, in order to avoid

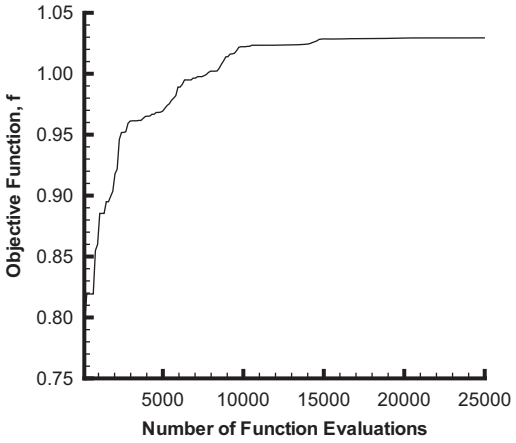

Fig. 11. Convergence history of PSO (Case 2).

the intensive computational expense of solving a mixed discrete-continuous optimization problem. Larger rotor diameters are often accompanied by greater hub heights, which has also not been considered in this paper.

The PSO algorithm is allowed to run for 25,000 function evaluations for Case 2. A higher number of function evaluations is allowed to compensate for the increase in the dimensionality of the problem (N additional design variables). Fig. 11 shows that the algorithm converges after approximately 15,000 function evaluations during which the power generated by the farm increases by 28.75%. The power generated by the optimum farm layout (3.569 W) is 41.11% higher than that generated by the original farm layout in the experiment (Fig. 5). The resulting rotor diameters, in this case, can be higher than the rotor diameters of the model-turbines used in the experiment ($D = 0.12$ m). Consequently, the maximum possible power generation, from a single turbine, is not restricted by the power curve shown in Fig. 4. The objective function, in this case, does not conform with the conventional definition of farm efficiency; the function can reach values higher than unity as shown in Fig. 11. The optimum farm layout is shown in Fig. 12, and the wind velocity approaching each turbine is shown in Fig. 13 (a). Figs. 13(b) and 14 present the power generated by each turbine and the rotor diameter of each turbine in the optimum wind farm, respectively.

The optimized farm design (as shown in Fig. 12) exhibits an interesting distribution of the approaching wind velocity (as shown in Fig. 13(a)) and of the power generated (as shown in Fig. 13(b)) in

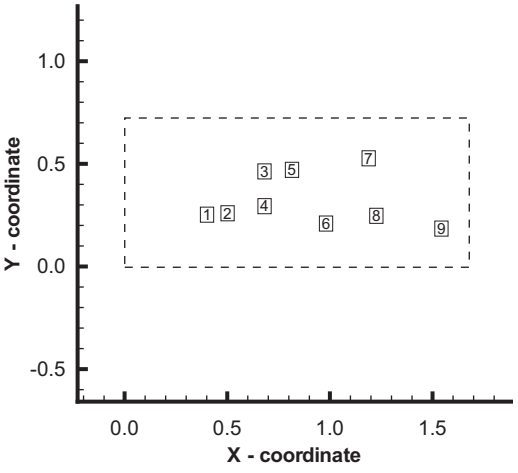

Fig. 12. Optimized wind farm layout in meters (Case 2).

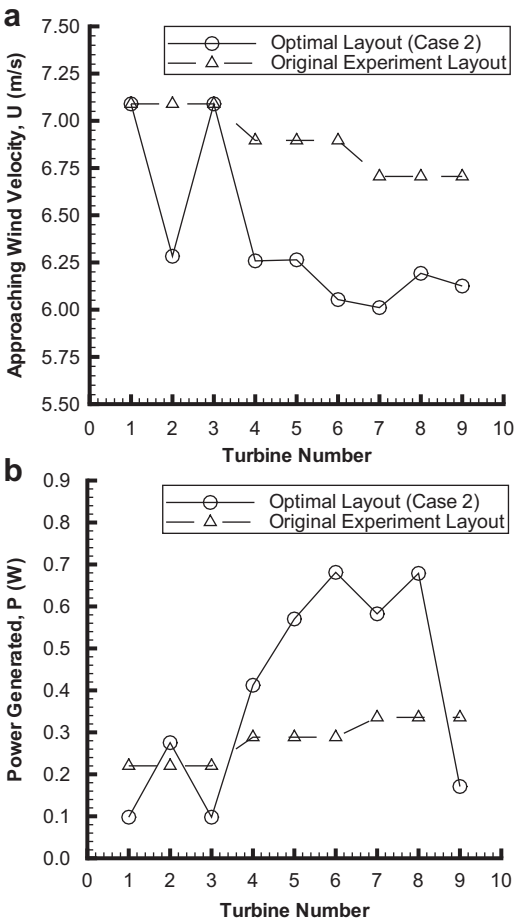

Fig. 13. (a) Velocity of wind approaching each turbine (U). (b) Power generated by each turbine (P).

the case of each turbine. Fig. 14 shows a significant variation in the rotor diameter of the turbines; the turbines with smaller rotors tend to be placed upstream of the turbines with larger rotors. The primary observation from the results of Case 2 is the remarkable increase in the total power generation, accomplished using non-identical turbines.

The rotor diameter has been considered as a continuous variable in this study; commercial wind turbines, however, present

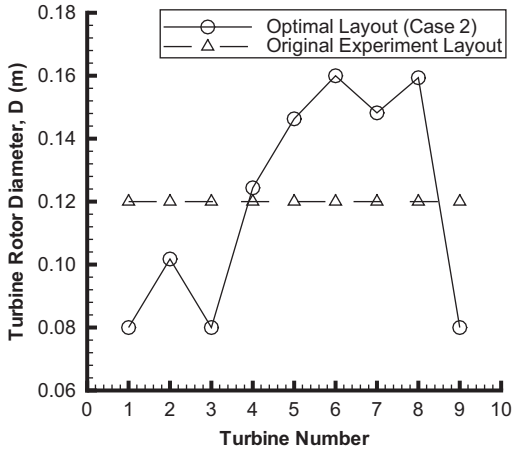

Fig. 14. Rotor diameter of each turbine (D) in the optimized wind farm (Case 2).

a discrete variation of the rotor diameter. Also, non-identical wind turbines might have different performance characteristics. In this case study, such data was not available and hence the same performance curves (as in Fig. 4) were used for all the turbines. In the case of a commercial wind farm, other design and economic factors might mitigate the cost benefit (cost reduction) of using differing rotor diameters. Owing to the above reasons, further research regarding use of differing rotor diameters needs to be undertaken that accounts for:

- the treatment of turbine rotor diameters as discrete variables,
- the specification of appropriate hub height (corresponding to different rotor diameters),
- the use of appropriate performance characteristics specific to each turbine, and
- the application of a comprehensive cost model.

6.5. UWFLO Case 3

Case 3 is designed to illustrate a more appropriate characterization of the commercial wind farm scenario. Modified power characteristics of the turbines are used in this case. Specifically, the power generated by a turbine is assumed to remain constant and equal to the rated power (of 0.385 W), when the approaching wind speed is above the rated speed (of 6.17 m/s). This change is introduced to better explain the effect of turbine wakes on the optimal layout of the wind farm. The incoming wind velocity is specified as 6.2 m/s to capture the more likely range of operation (with respect to wind speed) of the turbines. Other user-defined constants and parameters in this case are the same as in Case 1. On account of the above changes, the application of UWFLO to Case 3 is expected to produce a farm layout that minimizes the mutual shading effects of wind turbines.

Two parametric studies are also performed in Case 3. These studies investigate the effects of (i) the number of turbines in a farm, and (ii) the size of the farm, on the maximum power generation. Parametric Study-I (Section 6.6.1) applies UWFLO on five different wind farms, with the number of turbines equal to 6, 9, 12, 15 and 18, respectively. These wind farms have the same fixed dimensions, as in the experimental setup [15], which is $14D \times 6D$. The five different wind farms, analyzed in Parametric Study-2 (Section 6.6.2), are listed in Table 5. All the farms in Study-2 are assumed to be rectangular in shape, with a length to breadth ratio (X_{farm}/Y_{farm}) of 7/3.

6.6. UWFLO Case 3 results

PSO is run with the same user-defined constants as specified in Table 4. The farm layout obtained through optimization is shown in Fig. 15; the velocity of wind approaching each turbine and corresponding power generated are shown in Fig. 16 (a) and (b), respectively.

It can be observed, from the optimized layout shown in Fig. 15 that the nine wind turbines have been divided (by location) into two regions – (i) one, located at the front end of the wind farm with respect to the incoming wind, and (ii) the other, located at the rear end of the farm. Such a layout minimizes the shading effects, since the wake velocity deficit decreases with distance downstream from a turbine. This trend is also illustrated by the variation of the

Table 5
Parametric Study-II: Wind farms.

Farm	Farm dimensions ($X_{farm} \times Y_{farm}$)	Farm area (m^2)	Number of turbines
1	$7D \times 3D$	0.3024	18
2	$14D \times 6D$	1.2096	18
3	$21D \times 9D$	2.7216	18
4	$28D \times 12D$	4.8384	18
5	$35D \times 15D$	7.5600	18

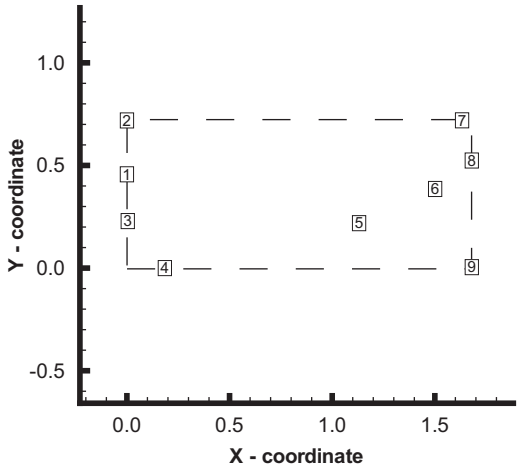

Fig. 15. Optimized wind farm layout in meters (Case 3).

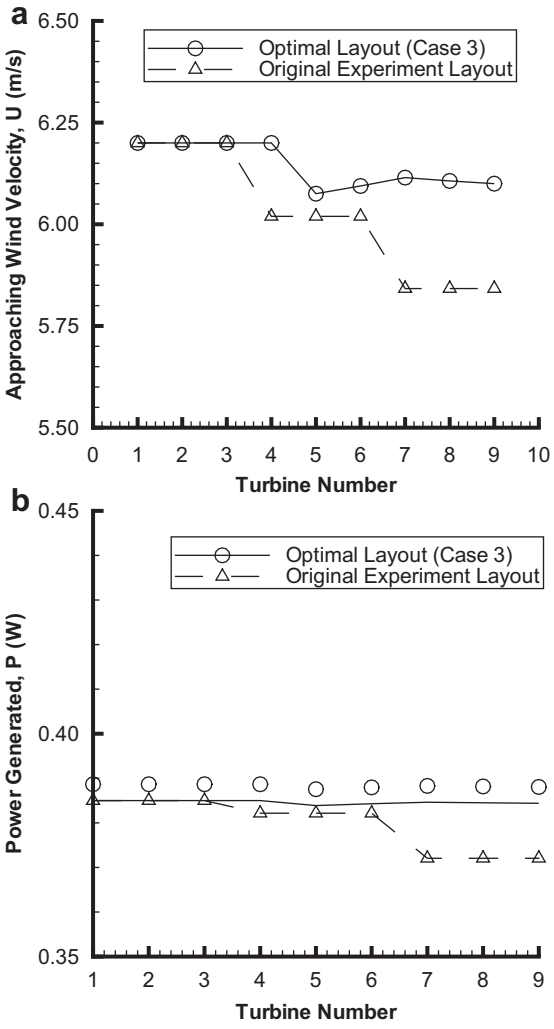

Fig. 16. (a) Velocity of wind approaching each turbine (U). (b) Power generated by each turbine (P).

approaching wind velocity, shown in Fig. 16(a). The turbines at the front end face the incoming wind at 6.2 m/s, and the turbines at the rear end face the wind approaching at a velocity of approximately 6.1 m/s. Hence, the power generated by the turbines (individually) at the rear end is also close to the rated power. However, if distributions of wind speed and direction are considered, the resulting optimized layout might be very different.

In the following sections, we will analyze the results of the two Parametric Studies (I and II). Studies I and II respectively investigate the influences of the number of turbines and of the farm land size on the maximum power (obtained through layout optimization) that can be generated by a wind farm.

6.6.1. Parametric study-I: fixed farm land size

In the case of a fixed size wind farm, the mutual shading effects of turbines are expected to become more pronounced with increasing number of operational turbines. The influence of this crowding effect on the farm efficiency, and thereby on the cost per KW of power produced, is investigated in this study. The cost per KW of power produced is evaluated using Eq. (22) in Section 3. The convergence histories of the application of UWFLO to the five wind farms are shown in Fig. 17. The farm efficiency and the cost per KW of power produced for each farm are illustrated in Fig. 18 (a) and (b), respectively. The farms efficiencies for Parametric Study-I are also summarized in Table 6. The farm number prefix (I- or II-) in column 1 of this table indicates which parametric study the wind farm corresponds to.

A higher number of turbines presents a higher dimensional (in design variable domain) problem, which demands more function evaluations during optimization; this phenomenon is shown in Fig. 17. Fig. 18(a) illustrates that the crowding effect (mutual shading of turbines) may significantly undermine the marginal increment in power with increasing number of turbines.

The most interesting observation is provided by the variation of the Cost per KW of power produced with increasing number of turbines. This variation is illustrated by Fig. 18(b), which indicates the existence of a minimum (for the cost at $N = 9$) with respect to number of turbines used. Hence, it is crucial to determine the optimal number of wind turbines in a farm, which ensures the lowest cost per KW of power production. Such information can be extremely beneficial in evaluating the genuine potential and profitability of a wind energy project. The planning of large scale wind farms involving hundreds of turbines can significantly benefit from such an analysis. Nevertheless, further investigation regarding the influence of the number of turbines is necessary in order to account for distributions of wind speed and direction that exist in the commercial scenario.

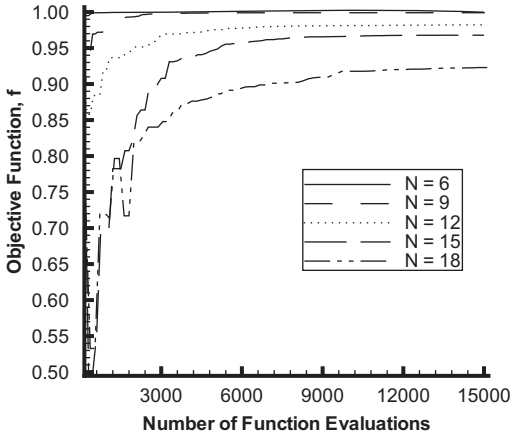

Fig. 17. Convergence history of PSO (Case 3, Study-I).

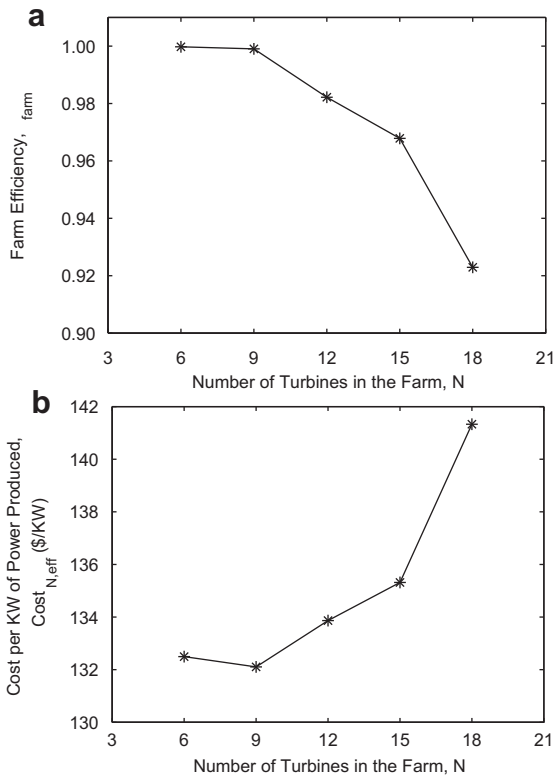

Fig. 18. (a) Farm efficiency. (b) Cost per KW of power produced.

6.6.2. Parametric study-II: fixed number of turbines

In the case of a fixed number of turbines, an increase in the farm land size is likely to reduce the mutual shading effect of turbines, and thereby enhances the farm efficiency. This phenomenon might also depend on the shape of the wind farm. In this paper, only rectangular wind farms have been studied. The convergence histories of the application of UWFLO to the five wind farms of different dimensions are shown in Fig. 19. Fig. 20 shows the variation of the farm efficiency (obtained through optimization) with increasing farm land size. In this figure, the horizontal axis represents the area of the wind farm (S_{farm}) as a multiple of the area of the smallest farm studied, which is given by

$$S_{\text{farm}} = \frac{X_{\text{farm}} \times Y_{\text{farm}}}{7D \times 3D} \tag{33}$$

The critical output parameters (for Parametric Study-II) are also summarized in Table 6.

It is readily observed from Fig. 20 that the farm efficiency increases with increase in the farm land size only to a certain level (which is $21D \times 9D$ in this study); beyond this level, there is no

Table 6
Case 3, Parametric Study results.

Farm	Farm dimensions ($X_{\text{farm}} \times Y_{\text{farm}}$)	Number of turbines	Farm efficiency after optimization
I-1	$14D \times 6D$	6	0.999
I-2	$14D \times 6D$	9	0.999
I-3	$14D \times 6D$	12	0.982
I-4	$14D \times 6D$	15	0.968
II-1	$7D \times 3D$	18	0.553
I-5/II-2	$14D \times 6D$	18	0.923
II-3	$21D \times 9D$	18	0.993
II-4	$28D \times 12D$	18	0.994
II-5	$35D \times 15D$	18	0.999

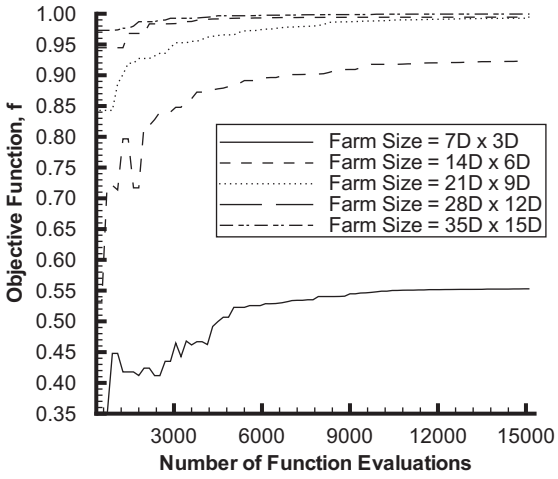

Fig. 19. Convergence history of PSO (Case 3, Study-II).

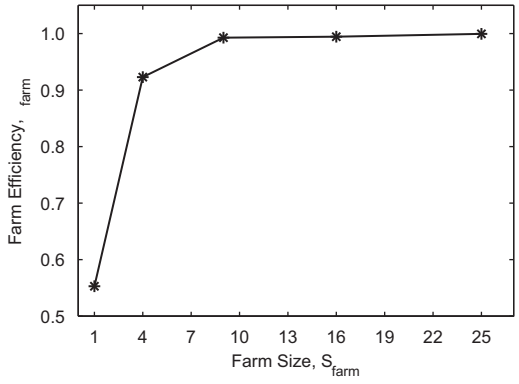

Fig. 20. Farm efficiency of wind farms with different number of turbines (Case 3, Study-II).

additional gain in the total power generated, by increasing the farm land size. Appropriate data for the cost of a wind farm land was not readily available; hence, we could not explore the variation of the cost of the optimized wind farm with respect to the farm land size. However, it is expected that a larger sized farm would generally demand a higher cost of land and an associated increase in the cost of Operation and Maintenance (O&M). These observations show that the determination of the optimum farm land size (for a wind energy project) is crucial to wind farm planning. However, from a commercial perspective, we also need to consider factors such as the availability of land at a particular site and the local terrain.

7. Conclusion

The Unrestricted Wind Farm Layout Optimization (UWFLO) model developed in this paper does not make typical limiting assumptions regarding the arrangement of turbines in a wind farm. In addition, it accounts for a velocity-based variable induction factor, and the partial overlap of wakes on a downstream turbine rotor. The associated power generation model is successfully validated against data measured in a wind tunnel experiment of a scaled down wind farm. The slight disagreement between the parameter values determined by the model and corresponding experimental data can be attributed to the standard assumptions made in the analytical wake model used in the paper. Layout optimization is performed on a wind farm, similar to that in the experiment. A significant increase (30% compared to the experimental farm) in the total power generation is realized. UWFLO was observed to configure the layout such that most of the turbines operate close to the maximum power point, given by the power curve. The constrained Particle Swarm Optimization (PSO) algorithm appositely dealt with the nonlinearity and the likely multimodality of the wind farm design problem.

The use of turbines with differing rotor diameters produced a remarkable increase in the total power generated by the farm, a 43% increase compared to the experimental farm. A cost constraint was applied to ensure that the use of non-identical turbines does not escalate the cost of the wind farm. Hence, the improvement in power generation highlights the potential benefits of using non-identical turbines in a wind farm. However, an appropriate consideration of the hub height, pertinent performance characteristics and a comprehensive cost model, is necessary to provide further insight in this direction. Additional parametric studies indicated that the selection of the optimal number of turbines, and the determination of the optimal farm land size are essential to planning an efficient wind farm. We can credibly conclude that the determination of the engineering-design requirements of a wind farm, namely number of turbines, type of turbines, and farm land size, can be accomplished through effective modeling and optimization, as presented in this paper. Such an approach can corroborate the prospects of wind becoming an important player in the future energy market.

Future developments in the UWFLO technique should account for the temporal variation in wind velocity, the local terrain, and other factors of commercial importance. Consideration of additional factors listed at the end of Section 6.4 will foster the exploration into the benefits of using multiple types of turbine in a wind farm. Further application of the UWFLO framework to a commercial scale wind farm would establish the true potential of this technique.

Acknowledgments

Support from the National Science Foundation Awards CMMI 0946765 and CMMI 1100948 is gratefully acknowledged. Valuable contribution from Jose Lebron, regarding the description and related data on the wind tunnel experiment, is also gratefully acknowledged.

References

[1] Burton T, David S, Jenkins N, Ervin B. Wind energy handbook. John Wiley & Sons; 2001.
[2] World wind energy report 2009. Tech. rep.. Bonn, Germany: World Wind Energy Association; March 2010
[3] Sorensen P, Nielsen T. Recalibrating wind turbine wake model parameters – validating the wake model performance for large offshore wind farms. In: European Wind Energy Conference and Exhibition, EWEA, Athens, Greece; 2006.
[4] Beyer HG, Lange B, Waldl HP. Modelling tools for wind farm upgrading. In: European Union Wind Energy Conference, AIAA, Goborg, Sweden; 1996.
[5] Jensen NO. A note on wind turbine interaction. Tech. Rep. M-2411. Roskilde, Denmark: Risoe National Laboratory; 1983.
[6] Katic I, Hojstrup J, Jensen NO. A simple model for cluster efficiency. In: European Wind Energy Conference and Exhibition, EWEA, Rome, Italy; 1986.
[7] Elkinton C, Manwell J, McGowan J. Offshore wind farm layout optimization (owflo) project: preliminary results. In: 44th AIAA Aerospace Sciences Meeting and Exhibit, AIAA, Reno, Nevada, USA; 2006.
[8] Ainslie JF. Development of an eddy viscosity model for wind turbine wakes. In: 7th BWEA Wind Energy Conference, BWEA, Oxford, UK; 1985. p. 61–66.
[9] Mosetti G, Poloni C, Diviacco B. Optimization of wind turbine positioning in large wind farms by means of a genetic algorithm. Journal of Wind Engineering and Industrial Aerodynamics 1994;54(1):105–16.
[10] Grady SA, Hussaini MY, Abdullah MM. Placement of wind turbines using genetic algorithms. Renewable Energy 2005;30(2):259–70.

[11] Sisbot S, Turgut O, Tunc M, Camdali U. Optimal positioning of wind turbines on gkeada using multi-objective genetic algorithm. Wind Energy 2009;13(4):297–306.
[12] Kusiak A, Zheng H. Optimization of wind turbine energy and power factor with an evolutionary computation algorithm. Renewable Energy 2010;35(3):1324–32.
[13] Gonzleza JS, Rodriguezb AGG, Morac JC, Santos JR, Payan MB. Optimization of wind farm turbines layout using an evolutive algorithm. Renewable Energy 2010;35(8):1671–81.
[14] Mikkelsen R, Srensen JN, ye S, Troldborg N. Analysis of power enhancement for a row of wind turbines using the actuator line technique, Journal of Physics: Conference Series 75(1).
[15] Cal RB, Lebron J, Kang HS, Meneveau C, Castillo L. Experimental study of the horizontally averaged flow structure in a model wind-turbine array boundary layer, Journal of Renewable and Sustainable Energy 2(1).
[16] Chowdhury S, Messac A, Zhang J, Castillo L, Lebron J. Optimizing the unrestricted placement of turbines of differing rotor diameters in a wind farm for maximum power generation. In: ASME 2010 International Design Engineering Technical Conferences & Computers and Information in Engineering Conference (IDETC/CIE 2010), no. DETC2010–29129, ASME, Montreal, Canada; 2010.
[17] Frandsen S, Barthelmie R, Pryor S, Rathmann O, Larsen S, Hojstrup J, et al. Analytical modeling of wind speed deficit in large offshore wind farms. Wind Energy 2006;9(1–2):39–53.
[18] Crespo A, Hernández J, Frandsen S. Survey of modelling methods for wind turbine wakes and wind farms. Wind Energy 1999;2:1–24.
[19] Kennedy J, Eberhart RC. Particle swarm optimization. In: IEEE International Conference on Neural Networks, no. IV, IEEE, Piscataway, NJ, USA; 1995. p. 1942–1948.
[20] Deb KK, Pratap A, Agarwal S, Meyarivan T. A fast and elitist multi-objective genetic algorithm: Nsga-ii. IEEE Transactions on Evolutionary Computation 2002;6(2):182–97.
[21] A. B. T. by D J Randall Introduction to the theory of flow machines. John Wiley & Sons; 1966.
[22] Lanchester FW. Contribution to the theory of propulsion and the screw propeller. Transactions of the Institution of Naval Architects 1915;57:98–116.
[23] Kiranoudis C, Voros N, Maroulis Z. Shortcut design of wind farms. Energy Policy 2001;29:567–78.
[24] Kaldellis JK, Gavras TJ. The economic viability of commercial wind plants in Greece a complete sensitivity analysis. Energy Policy 2000;28:509–17.
[25] Herman S. Probabilistic cost model for analysis of offshore wind energy costs and potential, Tech. Rep. ECN-I-02–007, Energy Research Center, Energy Research Center, Netherlands; May 1983.
[26] Jobs and economic development impact (jedi) model. Tech. rep. Golden, Colorado, USA: National Renewable Energy Laboratory; October 2009.
[27] Cockerill TT. Jobs and economic development impact (jedi) model. Tech. Rep. JOR3-CT95-0087. Sunderland, USA: Renewable Energy Centre, University of Sunderland; 1997.
[28] Zhang J, Chowdhury S, Messac A, Castillo L, Lebron J. Response surface based cost model for onshore wind farms using extended radial basis functions. In: ASME 2010 International Design Engineering Technical Conferences & Computers and Information in Engineering Conference (IDETC/CIE 2010), no. DETC2010–29121, ASME, Montreal, Canada; 2010.
[29] Kang HS, Meneveau C. Direct mechanical torque sensor for model wind turbines. Measurement Science and Technology 2010;21:105206.
[30] Hansen MOL. Aerodynamics of wind turbines. 2nd ed. London, UK: Eartsean; 2008.
[31] Lebron J, Castillo L, Cal RB, Kang HS, Meneveau C. Interaction between a wind turbine array and a turbulent boundary layer. In: 48th AIAA Aerospace Sciences Meeting including the New Horizons Forum and Aerospace Exposition, AIAA, Orlando, FL, USA; 2010.
[32] Colaco MJ, Orlande HRB, Dulikravich GS. Inverse and optimization problems in heat transfer, Journal of the Brazilian Society of Mechanical Science and Engineering 28(1).
[33] Chowdhury S, Dulikravich GS. Improvements to single-objective constrained predator-prey evolutionary optimization algorithm. Structural and Multidisciplinary Optimization 2010;41(4):541–54.